COMPARISON OF IMAGE ENHANCEMENT ALGORITHMS FOR IMPROVING THE VISUAL QUALITY OF POST-DISASTER SATELLITE IMAGES

B. Malvika, Student
Department of Electronics and Communication Engineering
Coimbatore Institute of Technology
Coimbatore, TN, 641 014, India
malvika.badri@gmail.com
Ramesh Sivanpillai, Senior Research Scientist
Department of Botany & WyGISC
University of Wyoming
Laramie, WY 82071, USA
sivan@uwyo.edu
B. Bhuvaneshwari, Assistant Professor
Department of Electronics and Communication Engineering
Coimbatore Institute of Technology
Coimbatore, TN, 641 014, India
bbhuvana.suresh@gmail.com

ABSTRACT

Remotely sensed imagery is used by emergency management agencies worldwide as part of disaster-response activities. The overall quality of many of these images can be poor if features such as haze and clouds are present during their acquisition. Under these circumstances enhancement algorithms can be used to improve image quality and their utility for identifying disaster impacted areas. There are numerous image enhancement techniques that range in complexity and time required to complete them. However, for the purpose of post-disaster response, these images have to be processed quickly without compromising their quality. In this paper, three image enhancement algorithms were tested on four satellite images to benchmark the time taken to process them and their output quality. Landsat images acquired in 2011 (Landsat 5 TM) and 2016 (Landsat 8 OLI) were used in this study. The algorithms range in their complexity and rely on global and local statistics. Results from this study would provide insights to image analysts for selecting image enhancement algorithms while processing post-disaster images.

KEYWORDS: Natural disasters, Emergency response, Disaster Charter, Landsat, Rapid mapping

INTRODUCTION

Satellite images acquired after disasters such as flooding, landslides and mudslides, wildfires, etc., are used by emergency management agencies to aid response activities (Tralli et al. 2005; Nourbakhsh et al. 2006; Voigt et al., 2007). Current conditions of disaster impacted areas can be extracted from post-disaster images and further changes, such as debris flow and burn severity, can be mapped through repeated observations. Through the International Charter on Space and Major Disasters (https://www.disasterscharter.org/), emergency management agencies can obtain satellite data at no-cost from 16 member agencies for mapping post-disaster conditions and use them to plan response and assistance activities (Stryker and Jones 2009). These images have to be processed rapidly for extracting information about the impact and delivered to emergency management agencies.

However, presence of clouds, dust, smoke, and other particulate matter in the multispectral images collected by optical sensors reduces their quality (Sivanpillai, 2014; Shen et al. 2015; Lee and Lin 2016) and utility for disaster response activities. Chances of acquiring images with atmospheric obstructions are often higher during floods, landslides, and mudslides due to the presence of clouds and their shadows. As a result, mapping flooded and impacted areas in post-flood images can be difficult due to poor contrast or other impairments. Resources used for collecting these time-sensitive images from satellites and pre-processing them will be wasted if the necessary information cannot be extracted by emergency management agencies.

Data collected by active sensors (RADARSAT, TERRASAR, and ALOS) can be used for acquiring images for geographic areas covered by clouds (Peng et al. 2002). This can be useful for regions such as the tropics and mountains

that are covered by clouds for longer duration. However, interpreting and extracting information from multispectral data is relatively easier compared to the RADAR images. With multispectral data, it is possible to use visible and false color infrared band combinations to highlight different features in the image.

Numerous image enhancement algorithms exist for improving the quality of images acquired under cloudy or other conditions. Analysts can choose from algorithms that range from simple techniques such as histogram equalization to relatively complex ones such as the contrast limited adaptive histogram equalization (CLAHE). Input parameters for these algorithms vary from very minimal to relatively extensive. The time taken to process an image can also vary depending on the algorithm. The overall quality of the resultant images can be different based on the type of algorithm used and the input parameters specified. However, for post-disaster response these satellite images have to be processed relatively quickly without compromising their overall quality. Personnel in emergency management agencies have very limited time for processing these images and delivering the map products to those who are involved in rescue efforts.

Given that numerous image enhancement algorithms are available, it is not feasible to evaluate all of them to determine their suitability during emergency response operations. The primary objective of this study is to evaluate a suite of commonly used image enhancement algorithms on several post-flood satellite images. In the first phase of this study, three image enhancement algorithms (histogram equalization, contrast stretching, and contrast limited adaptive histogram equalization) were tested on four post-flood Landsat images to benchmark the output image quality and the time taken to process them. Results from this study will provide valuable insights to image analysts for selecting an image enhancement algorithms for processing post-disaster images during an emergency.

MATERIALS AND METHODS

Landsat data

Four Landsat sub-scenes were used in this comparison study (Figure 1). Two sub-scenes were extracted from Landsat 5 Thematic Mapper data acquired on 3 May 2011 (WRS2 Path: 22; Row 34), and another two sub-scenes were extracted from Landsat 8 Operational Land Imager (OLI) data acquired on 20 March 2016 (WRS2 Path 23; Row 38).

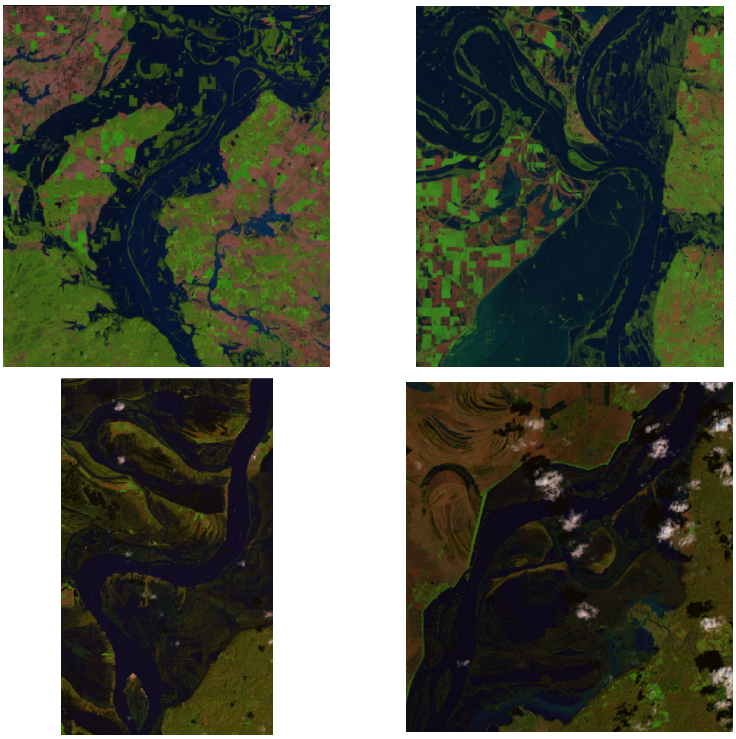

Figure 1: Landsat 5 TM images (top row) and 8 OLI images (bottom row) displayed in natural color (NIR2, NIR1, and Green in RGB) that were used for comparing three contrast stretch enhancement algorithms.

Landsat scenes were processed by the US Geological Survey to the level 1 terrain corrected (LIT) level. Band designation and wavelength ranges for the four bands included in this study are listed in Table 1, and information for all bands can be obtained from http://landsat.usgs.gov. Pixel digital numbers (DNs) were used in this study. Landsat 5 TM image was in 8 bit format while the 8 OLI image was in 16 bit format, and the spatial resolution of both data were 30 m for the four bands included in this study.

Table 1. Band designations and wavelength ranges of the four bands included in this comparison study

Landsat 5		Landsat 8	
0.45 – 0.52 µm	Band 1 – Blue	0.45 – 0.51 µm	Band 2 - Blue
0.52 – 0.60 µm	Band 2 – Green	0.53 – 0.59 µm	Band 3 - Green
0.76 – 0.90 µm	Band 4 – NIR1	0.85 – 0.88 µm	Band 5 – NIR
1.55 – 1.75 µm	Band 5 – NIR2	1.57 – 1.65 µm	Band 6 - SWIR

Contrast enhancement methods

The primary objective of contrast enhancement (CE) methods is to increase the overall visibility of the different earth surface features in the satellite images. Radiance values of the earth surface features vary widely from very dark to very bright hence the dynamic range of sensors must be designed to accommodate them (Schowengerdt, 2006). However the geographic area captured in any image might not include the full range of radiance values. When these images are displayed in a device such as a computer monitor, they will be confined to a narrow range resulting in low contrast (Jensen, 1996). Several CE techniques exist to improve the visual quality of remotely sensed images. In this study we selected three CE techniques that are available in many image processing software packages to benchmark the processing time and the quality of the output images.

Histogram equalization (HE)

Histogram equalization is a non-linear CE algorithm that computes the statistics for each spectral band, and then reassigns the pixels throughout the entire range of values resulting in a more or less flat histogram (Schowengerdt, 2006). The resultant image will have higher contrast where most pixels were populated in the original histogram. On the other hand, the tails of the original histogram will have reduced contrast (Jensen, 1996). This algorithm requires the analyst to specify the number of output values and the spectral bands. This algorithm is available in almost all commercially available image processing software.

Standard deviation stretching (SDS)

Standard deviation stretching is a linear CE algorithm that reassigns the pixels from a narrow range to the entire range of values available in a display device. Different methods are used to stretch these pixel values based on the histogram of pixel values in the original image. A standard deviation stretch is one of the contrast stretching methods in which the analyst specifies the value for the standard deviation from the mean (Jensen, 1996). Pixels below and above the specified standard deviation will be reassigned to minimum (0) and maximum of the display device (e.g., 255 in most computer monitors). Rest of the pixels will be linearly stretched between the minimum and maximum values. The SDS method requires to start with any random standard deviation value and increased in increments until a good quality output is obtained. In this study we started with the standard deviation of 1.0, and increased it by increments of 0.02.

Contrast Limited Adaptive Histogram Equalization (CLAHE)

CLAHE is a type of local contrast enhancement technique that is not influenced by the presence of outliers i.e., extremely high or low pixel values in the image. Local contrast enhancement methods such as adaptive histogram equalization (AHE) uses information from a small region surrounding each pixel for changing its value (Pizer et al. 1987). CLAHE is an improvement of AHE in terms of how the shape of the histogram is defined, and often produces images with better quality (Yadav et al. 2014). The image is divided into an analyst specified number of tiles, and histogram equalization is performed for each region after clipping a small portion of the histogram before computing the cumulative

distribution function (Park et al. 2008). For CLAHE, the analyst experimented with different tile sizes such as [16 16], [12 12], [8 8], [4 4], and [2 2], and clipping limit of 0.08, 0.05 and 0.02.

Bands corresponding to the blue, green, NIR1, and NIR2 (SWIR for Landsat 8) regions of the spectrum were processed in MATLAB (version R2016a) installed in a laptop computer with Intel Core i3, 2.00 GHz, 64-bit processor with 4GB RAM. Each band was processed independently and the parameters recorded at the end of each method include

a) Time taken (seconds/file size in GB), &

b) Mean, standard deviation, and range values of the bands in the enhanced images.

RESULTS AND DISCUSSION

HE processed all the images faster than SDS and CLAHE (Table 2). CLAHE needed most time to process the images. Processing 16-bit Landsat 8 OLI data required approximately twice more time than processing the 8-bit Landsat 5 TM data. It might not be appropriate to scale these processing times linearly for estimating the time to process an entire Landsat scene. However these results indicate that CLAHE algorithm would require more time to process the image.

Table 2. Time taken to process the Landsat images By the three enhancement algorithms selected for this study

Image	Histogram Equalization	Std. Deviation Stretch	CLAHE
Landsat 5 – TM (1)	3 sec/GB	5 sec/GB	21 sec/GB
Landsat 5 – TM (2)	2 sec/GB	4 sec/GB	38 sec/GB
Landsat 8 – OLI (1)	4 sec/GB	7 sec/GB	69 sec/GB
Landsat 8 – OLI (2)	5 sec/GB	8 sec/GB	55 sec/GB

Enhanced images displayed in natural color combination (NIR2/SWIR in Red, NIR1 in Green, and Green in Blue) were visually superior to their corresponding true color combination images. Therefore results from the natural color combinations are included in this section.

In terms of the analyst input, HE required no input and all four output images had high contrast (Figures 2 and 3, column 1). However saturation was evident in the enhanced Landsat 8 – OLI natural color images, resulting in loss of information (Figure 3, column 1). Presence of clouds in these images could have resulted in the saturation of several pixels. We found that around standard deviation of 2.0 from the mean produced visually good quality results (Figures 2 and 3, column 2). When the value of the standard deviation from mean was 1 (starting value), the output image appeared white. When the value increased, the output image appeared dark, i.e., closer to the original image. However the time taken to process the images remained the same for all standard deviation values.

Table 3. Summary statistics of spectral bands 5, 4, 2 of Landsat 5 TM images

Image	Mean	Standard Deviation	Range	Mean	Standard Deviation	Range	Mean	Standard Deviation	Range
Landsat 5 – TM(1)	NIR2 (Band 5)			NIR1 (Band 4)			Green (Band 2)		
Original	56	38	253	65	35	169	39	7	127
HE	128	74	251	128	74	251	131	73	243
SDS	109	80	253	112	76	253	105	65	245
CLAHE	100	70	254	103	68	254	78	75	198
Landsat 5 – TM(2)									
Original	37	33	254	54	34	168	39	5	129
HE	129	74	247	130	73	247	128	74	251
SDS	84	81	252	83	76	253	126	61	241
CLAHE	80	66	254	93	65	254	72	25	192

For CLAHE method in natural color images, [8 8] tile size with clipping limit of 0.02 produced visually high quality results (Figures 2 and 3, column 3). At higher tile sizes, the contrast decreased and the output image appeared darker. When the tile size was lower [4 4], [2 2], the output image became brighter, i.e., too much contrast. Similarly, when increasing the clipping limit from 0.02, the quality of output images decreased (became noisier). Similar to the standard deviation stretch, the time taken to complete the processing remained the same for all combinations of tile sizes and clipping limit values.

Mean pixel value, its standard deviation and range for all the bands were higher than the original Landsat TM and OLI bands (Tables 3 & 4). Among the three enhancement methods, the standard deviation values of the bands generated through CLAHE were lower except for the Landsat 5 TM (1) green band (Tables 3 & 4). Examining the histograms of the enhanced bands indicated that the range of spectral values were wider than the original bands.

Table 4. Summary statistics of spectral bands 6, 5, 3 of Landsat 8 OLI images

Image	Mean	Standard Deviation	Range	Mean	Standard Deviation	Range	Mean	Standard Deviation	Range
Landsat 8 – OLI (1)	SWIR (Band 6)			NIR (Band 5)			Green (Band 3)		
Original	7997	2497	25234	8870	2538	29061	8625	779	29061
HE	32634	19209	64495	33065	19006	64495	33180	18794	64495
SDS	22019	18662	65527	21952	17732	65528	30098	17487	65507
CLAHE	17765	10104	52135	18490	10375	54537	13719	3499	32171
Landsat 8 – OLI (2)									
Original	9949	4217	33267	10635	3950	38621	9276	2202	31384
HE	32745	19149	63455	33344	18871	63455	33311	18839	64495
SDS	22350	17890	65530	20070	15527	65531	14476	10862	65528
CLAHE	21306	13050	59709	21661	11994	62055	15571	5493	48949

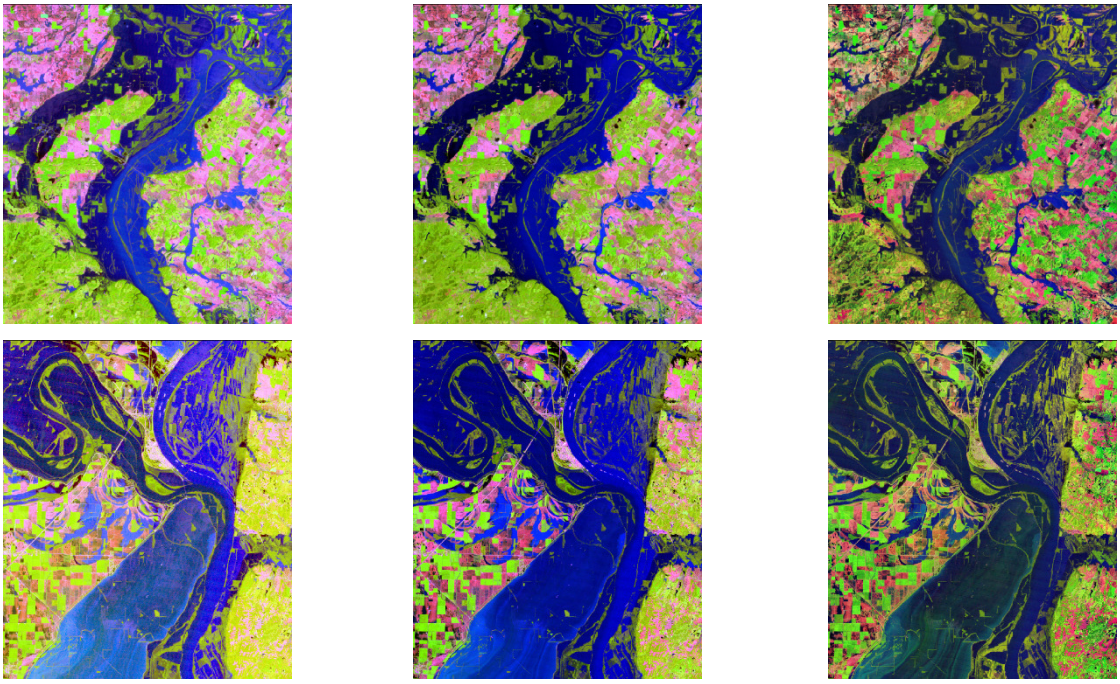

Figure 2. Enhanced Landsat 5 TM images (rows 1 & 2) derived from Histogram equalization - HE (column 1), Standard deviation stretch - SDS (column 2), and CLAHE (column 3).

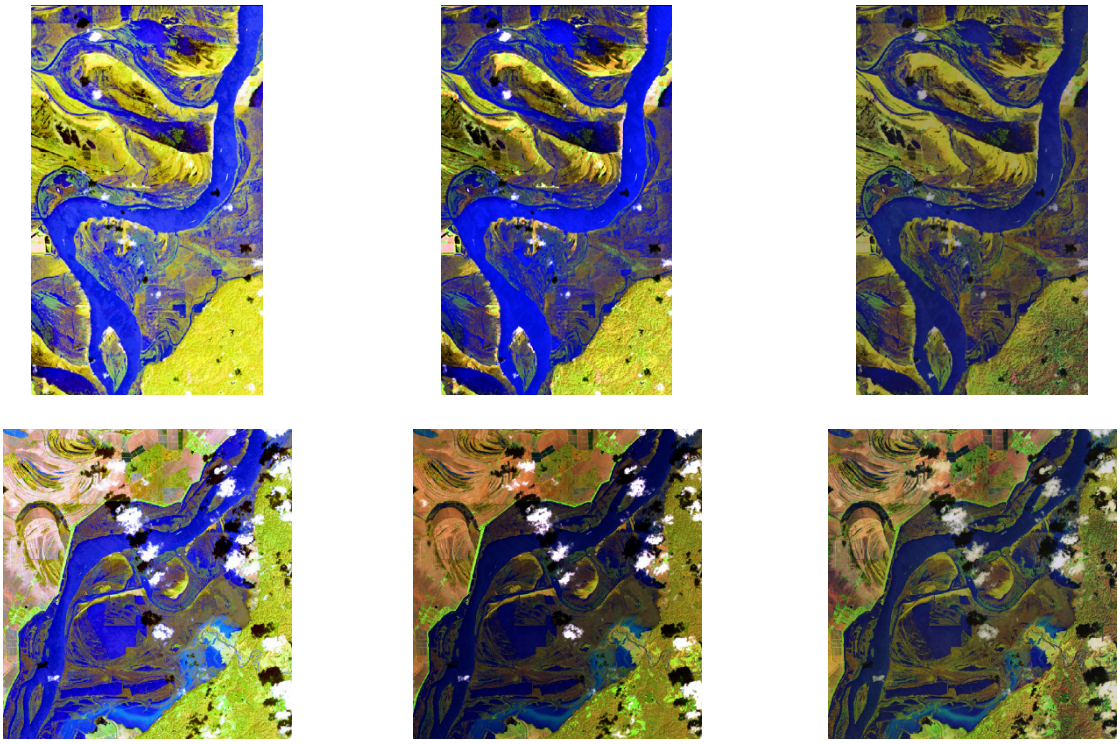

Figure 3. Enhanced Landsat 8 OLI images (rows 1 & 2) derived from histogram equalization – HE (column 1), standard deviation stretch – SDS (column 2), and contrast limited adaptive histogram equalization (column 3).

Based on these results, we can conclude that the enhanced images derived from CLAHE were of better quality, though it took longer (approximately 12 times) to process them. Output images had fewer saturation-related issues and the earth surface features were distinguishable in the images with the presence of clouds. Though the processing time was lower in HE and SDS, there is an increased risk of obtaining saturated pixels in the output image which could result in lost information. However, the additional processing time needed to complete the CLAHE could be an issue when the number of images are higher.

FUTURE WORK

In the second part of this research project, we will include three additional image enhancement algorithms for processing these Landsat images. We will add satellite images collected from ASTER and MODIS satellites which are also used for emergency response operations. In the third and final part of this project, we will benchmark these algorithms for different computing platforms (desktops and servers) and compare the time taken to complete each enhancement. Insights gained from our study will help analysts select algorithms during future emergency response operations.

ACKNOWLEDGEMENT

We gratefully acknowledge the travel support provided to the second author by the Center for Global Studies and the Haub School of Environmental and Natural Resources at University of Wyoming. We thank Dr. A. Rajeswari, Professor and Head, Department of Electronics and Communication Engineering, Coimbatore Institute of Technology, for her support.

REFERENCES

Jensen, J.R., 1996. *Introductory digital image processing: A remote sensing perspective*, Third Edition. Upper Saddle River, New Jersey, Prentice Hall Inc.

Lee, K-Y., C-H, Lin. 2016. Cloud Detection of Optical Satellite Images Using Support Vector Machine. International Archives of the Photogrammetry, Remote Sensing and Spatial Information Sciences., XLI-B7:289-293, DOI:10.5194/isprs-archives-XLI-B7-289-2016.

Nourbakhsh, I., R. Sargent, A. Wright, K. Cramer, B. McClendon, and M. Jones, 2006. Mapping disaster zones, *Nature* 49:787-788. DOI: 10.1038/439787a.

Peng, X., J. Wang, M. Raed, and J. Gari., 2002. Land cover classification using RADARSAT data in a mountainous area of southern Argentina. *Proceedings from the Geoscience and Remote Sensing Symposium*, Jun 24-28, 2002. DOI: 10.1109/IGARSS.2002.1027152.

Pizer, S.M., E.P. Amburn, J.D. Austin, R. Cromartie, A. Geselowitz, T. Greer, B. t. H. Romeny, J. B. Zimmerman, and K. Zuiderveld, 1987. Adaptive histogram equalization and its variations. *Computer vision, graphics, and image processing*, 39: 355-368.

Richards, J.A., X. Jia., 1999. Remote sensing digital image analysis: An introduction, 3rd edition, Springer, Berlin, 363p.

Schowengerdt, R.A., 2006. *Remote sensing: models and methods for image processing*. Second Edition, London, Academic Press.

Shen, X., Q. Li., Y. Tian, L. Shen. 2015. An Uneven Illumination Correction Algorithm for Optical Remote Sensing Images Covered with Thin Clouds. *Remote Sensing,* 7:11848-11862. DOI: 10.3390/rs70911848.

Sivanpillai, R., 2014. Remotely Sensed Images for Flood Monitoring: Lessons Learned from the 2011 Midwestern US Floods. Abstract NH11B-3699. *Proceedings of the 2014 AGU fall meeting,* Dec 15-19, 2014.

Stryker, T., and B. Jones 2009. Disaster Response and the International Charter Program. *Photogrammetric Engineering and Remote Sensing*, 1342-1344.

Tralli, D.M., R.G. Blom, V. Zlotnicki, A. Donnellan, and D.L. Evans, 2005. Satellite remote sensing of earthquake, volcano, flood, landslide and coastal inundation hazards. *ISPRS Journal of Photogrammetry & Remote Sensing* 59:185-198. DOI: 10.1016/j.isprsjprs.2005.02.002

Voigt, S., T. Kemper, T. Riedlinger, R. Kiefl, K. Scholte, and H. Mehl, 2007. Satellite Image Analysis for Disaster and Crisis-Management Support. *IEEE Transactions on Geoscience and Remote Sensing*, 45(6): 1520 – 1528. DOI: 10.1109/TGRS.2007.895830.

Yadav, G., S. Maheshwari, and A. Agarwal., 2014. Contrast limited adaptive histogram equalization based enhancement for real time video system. *Proceedings from the 2014 International Conference on Advances in Computing, Communications and Informatics*, Sept.24-27, 2014. DOI: 10.1109/ICACCI.2014.6968381.